Supershells in metal clusters

H. Nishioka
Department of Physics, Konan University, 8-9-1 Okamato, Higashinada-ku, Kobe 658, Japan and The Niels Bohr Institute, University of Copenhagen, DK-2100 Copenhagen Ø, Denmark

Klavs Hansen
Tandem Accelerator Laboratory of The Niels Bohr Institute, DK-4000 Roskilde, Denmark

B. R. Mottelson
Nordisk Institut for Teoretisk Atomfysik (NORDITA), DK-2100 Copenhagen Ø, Denmark
(Received 5 April 1990)

Assuming a spherical mean field for electrons in metal clusters, single-particle level densities and electronic binding energies are calculated for clusters with up to 4000 valence electrons. Two phenomenological mean-field potentials, simulating microscopically calculated ones, are used. A global beating pattern, which envelopes individual shell oscillations, emerge from the calculations. The semiclassical interpretation of such a supershell structure, as proposed by Balian and Bloch in terms of interference of amplitudes associated with classical closed orbits, is found to be valid in the present case. Thermal effects, which tend to smear out shell and, therefore, supershell structures, are investigated qualitatively. Consequences of the shell structure are not obscured for cluster sizes up to several thousand atoms under the experimentally accessible temperature of 100–1000 K.

I. INTRODUCTION

For several years the properties of atomic and molecular clusters have attracted considerable interest. This is to a great extent due to the fact that the properties of clusters do not in general vary smoothly between the isolated atom or molecule and the bulk. One of the most striking manifestations of this nonuniform approach to the bulk is the variations in the abundance of clusters with different mass numbers, when produced, e.g., in a supersonic expansion or by sputtering.[1,2]

The abundance spectra show pronounced peaks for clusters composed of metal atoms as well as for nonmetal elements, albeit at different mass values for the two kinds of cluster. Whereas the peaks in the abundance spectra for clusters composed of nonmetal elements can be explained by reference to certain geometrical configurations of the atoms in the cluster, the explanation in the case of metal clusters is related to the quantized motion of the valence electrons within the entire cluster volume.

The "magic numbers" for metal clusters were first observed by Knight *et al.* (for sodium[3]) and by Katakuse *et al.* (for silver[4]) and were shown to be analogous to "magic numbers" for nuclei.[5] For the nuclei these numbers correspond to the numbers of neutrons and protons at which nuclei are particularly stable, and the investigation of stability versus particle number led to an understanding of the shell structure in nuclei.[6] It was realized that the "magic numbers" reflect shell closings arising from the quantization of the motion of delocalized fermions in a mean-field potential of high symmetry.

The mean-field potential of nuclei is observed to be almost constant ($\simeq -50$ MeV) in the interior and to vanish smoothly at the surface of the nuclei. Neglecting the spin-orbit coupling, which is very small in clusters of lighter elements, such a potential produces shell closings at particle numbers $N=2,8,20,34,40,58,92$. These are precisely the number of electrons in the metal clusters for which the mass spectra exhibit local maxima.

The shell closings were found not only in the abundance spectra but also later for the static polarizability[7] and in the ionization potentials[8] (although the magnitude of the effect for the ionization potential is smaller than anticipated). There is, therefore, very little doubt that an important part of the ground-state energy of (alkali-metal) clusters with a number of atoms $N \lesssim 10^2$ is determined by the motion of the valence (or conduction) electrons and that these can be considered to move in a common mean-field potential similar to the potential experienced by a nucleon in a nucleus.

The discovery of quantal shells in metal clusters establishes illuminating connections between this field of research and the studies of atoms and nuclei which are also dominated by shell structure. In addition the discovery opens completely new possibilities for investigations of shell structure in systems with particle number N sufficiently large so as to reveal the characteristic structure expected in the semiclassical limit. With atoms and nuclei there is a natural upper limit of particle number N. With metal clusters there is no such upper limit. In principle N can be varied from 1 to ∞, so that investigation of changes in properties from atomic levels to bulk metals, characterized by band structure, should be possible. There are indeed current experimental efforts[9] to extend the measurements to large magic numbers.

The shell structure, or the quasiperiodic oscillation of the single-particle level density, tends to die out gradually as N becomes larger. In a spherical potential, however,

the decrease in amplitude of the oscillation for a given value of N relative to the monotonous average level density is of the order $N^{-1/6}$ (Ref. 10). It is still 30% in the $N=10^3$ region, and does not exclude the possibility of observing shell effects for clusters up to, at least, this size range.

Balian and Bloch have shown[11] that the single-particle level density for a spherical cavity behaves in a very characteristic way. As a function of energy (or momentum) the level density shows a global long-wavelength oscillating pattern that envelopes short-wavelength periodic oscillations, each corresponding to an ordinary shell. We associate these long-range oscillations with "supershells." Balian and Bloch have clarified the origin of the supershells in a simple and beautiful way through a semiclassical treatment of the single-particle level density. The supershell is the beating pattern of two interfering waves associated in the semiclassical treatment with triangular and square closed orbits inside the cavity. The neighboring shell spacing in momentum is proportional to the inverse of the length of the shortest orbit (triangle), while the supershell spacing is proportional to the inverse of the length difference between the two orbits, which is ~ 11 times the shell spacing.

Despite its beauty Balian and Bloch's work has not received much attention in the 18 years that have elapsed since it appeared. This is because one period of the supershell encompasses a number of single-particle levels of the order of 10^3. As a consequence, this work was often considered to be a purely theoretical exercise of little relevance for the description of realistic quantum systems on the earth or elsewhere in the universe. The discovery of shell structure in metal clusters has brought new attention to their work, since now the supershell has become a phenomenon that can be investigated experimentally as well as theoretically.

The spherical cavity used by Balian and Bloch in order to illustrate the supershell is too simple to allow realistic predictions of the level densities in metal clusters. On the other hand, self-consistent calculations of the mean-field potentials for metal clusters using the spherical and homogeneous jellium model as an approximation to the distribution of the positively charged ions give an almost constant value for the potential inside the cluster and a smoothly and rapidly increasing surface part.[12,13] This leads us to expect that the results obtained with the spherical cavity are not entirely without relevance to metal clusters; we expect supershells to appear also with more realistic potentials.

In this paper we present the results of level-density and binding-energy calculations for electrons in potentials that simulate the self-consistent mean-field potentials derived by Ekardt for Na clusters.[12] The potentials are given in Sec. II. The results given in Secs. III–V show that there are indeed supershells in Na clusters, provided that the mean field is still a valid concept for clusters containing 1000 or more atoms. In these sections we also investigate the level densities semiclassically and prove that Balian and Bloch's interpretation of the supershells in terms of the closed orbits is valid for the metal clusters.

There are, however, several aspects to the cluster structure and their production processes that set limits to the observation of shell structure, and therefore, of the supershells. We shall make qualitative investigations of such finite-temperature effects in Sec. VI.

II. MEAN-FIELD POTENTIALS FOR VALENCE ELECTRONS

The Kohn-Sham density-functional method[14] is one of the most practical and also successful methods for calculating electronic properties of metals. Within the Kohn-Sham framework, the jellium approximation to the positively charged ionic background has given quantitative agreement not only with bulk properties, but also with the measured surface energies of alkali metals (except for lithium).[15] Recently this self-consistent jellium model has been applied to metal clusters, especially to Na clusters.[12,13]

Effective local mean-field potentials for the valence electrons were calculated assuming a spherical distribution of the ionic background with uniform density equal to that of bulk sodium metal. The measured magic numbers were verified by the calculated ionization potentials, displaying maxima at shell closings and thus indicating relatively high stability of clusters with closed shells.[16] Ekardt[12] also calculated the effective mean-field potentials for particle numbers corresponding to a complete filling of each orbit up to $N=198$. The general properties of these potentials are, first, almost uniform depth of the inner part, and second, a universal shape of the smoothly vanishing surface part. There are small deviations from the uniform depth of the inner part, which make the bottom of the potential wavy. These deviations show no systematic behavior except for a small dip near the surface, and become smaller as N increases. We shall assume that their effects on the shell and supershell structures are of minor importance so that they can be neglected.

Ekardt's potentials will here be approximated by a simple three-parameter analytic expression in terms of a spherical Woods-Saxon potential:

$$U(R)=\frac{V_0}{1+\exp[(R-R_0)/a_0]}\ , \tag{2.1}$$

with parameter values

$$\begin{aligned} &V_0=-6.0\ \text{eV}\ , \\ &R_0=r_0N^{1/3},\quad r_0=2.25\ \text{Å}\ , \\ &a_0=0.74\ \text{Å}\ . \end{aligned} \tag{2.2}$$

The quantity V_0 is the depth of the potential, R_0 is the radius, and a_0 is the surface thickness, whereas R is the radial coordinate. The potential (2.1) vanishes faster than Ekardt's as R exceeds R_0. Still, the Fermi energy is 3 eV (half of the total depth of the potential) as it should be, and the single-particle wave functions of the occupied states extend only slightly into the region $R>R_0$. Therefore the small difference at $R>R_0$ is not a serious problem for the calculation of the orbits occupied in the ground-state configuration. The value of r_0 in Eq. (2.2) is slightly larger than the Wigner-Seitz radius for bulk sodi-

um (2.08 Å). This is due to the so-called "spill out" resulting from the extension of the electrons into the region outside the positive charge. As N increases r_0 should eventually approach the Wigner-Seitz radius. This slight dependence of r_0 on N is neglected in our calculations, because its effect should be of minor importance for the phenomena considered in the present work.

We also explore another type of potential, which was obtained through a semiclassical approximation[17] applying the Kohn-Sham density-functional method to a positive jellium background. In this approximation the density of the occupied electrons is expressed by a smooth three-parameter profile function which is determined variationally by requiring a minimum energy in the Kohn-Sham procedure. (For details see Ref. 17.) Figure 1 compares this potential (solid curve) with the Woods-Saxon potential (dotted curve) for $N=1000$. The inner part is slightly shallower and the outer part is deeper than the Woods-Saxon potential. A potential of this shape is called a "wine-bottle" potential in nuclear physics, and we will adopt this name in the following.

The "wine-bottle" potential has the advantage of reproducing the shallow minimum of Ekardt's potential in the surface region. On the other hand, the validity of the semiclassical approximation for metal clusters is still to be demonstrated.[18] All in all, it is difficult to know which of the two potentials is more realistic. In the following numerical studies we shall therefore use these two types of potential without any preference of one over the other. In doing so we are able to investigate effects on the shell and supershell structures coming from small differences in the potentials.

III. LEVEL DENSITIES IN THE WOODS-SAXON POTENTIAL

A. Quantum-mechanical calculation

The calculation of the single-particle level energies is performed by solving the radial wave equation numerically from the origin and identifying the solutions where the wave function vanishes smoothly, with the proper asymptotic form, for large distances.[19]

As in the case of the spherical cavity,[11] we plot the level density as a function of the wave number k rather than of the energy. Then the shell peaks appear approximately equally spaced in k, with the separation $\Delta k = 0.5 N^{-1/3}$ Å^{-1}.

Since the Woods-Saxon potential has a flat bottom, the wave number k is defined in a natural way as

$$k = \frac{1}{\hbar}[2m(E - V_0)]^{1/2} , \tag{3.1}$$

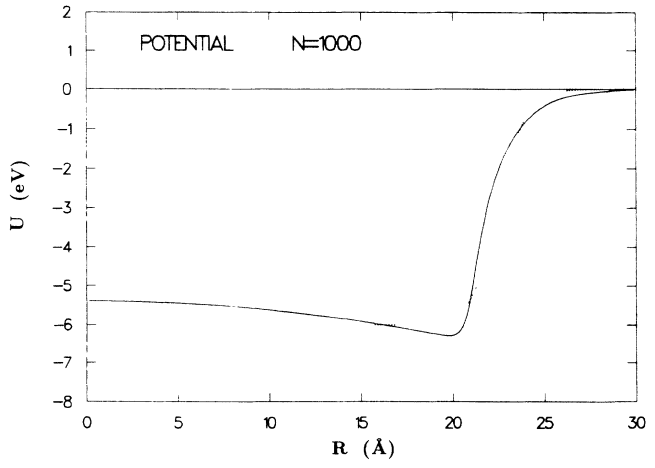

FIG. 1. Comparison of the Woods-Saxon potential (solid curve) and the wine-bottle potential (dotted curve) with $N=1000$.

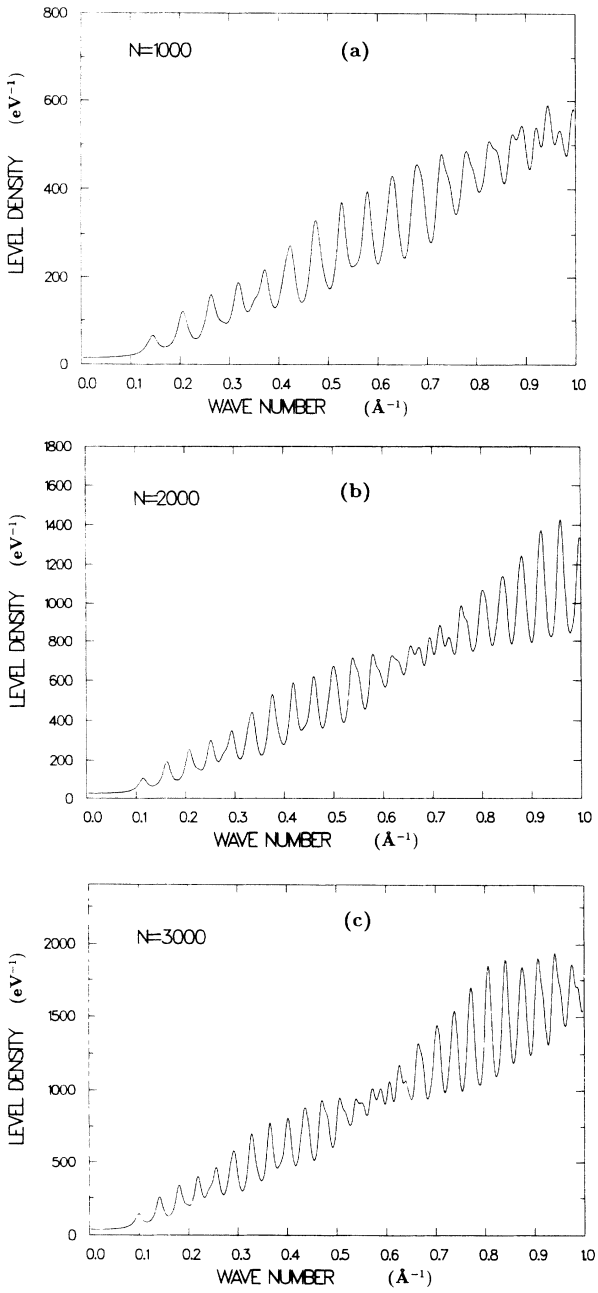

FIG. 2. Single-particle level densities in the Woods-Saxon potential with $N=1000$, 2000, and 3000 for (a), (b), and (c), respectively.

where m is the electron mass and V_0 is the depth of the potential ($V_0=-6.0$ eV).

For each single-particle binding energy E_{nl} a wave number k_{nl} is defined by Eq. (3.1). In order to visualize the shell and supershell structures clearly, we use the formal method of adding an imaginary part k_i to each k_{nl}. Instead of a sequence of δ functions, the level density is then smeared out and is given by

$$\rho(E)=\frac{2m}{\hbar^2}\sum_{n,l}\frac{2(2l+1)}{\pi}\frac{2k_ik_{nl}}{(k^2-k_{nl}^2)^2+(2k_ik_{nl})^2}\ . \tag{3.2}$$

The k_i is chosen to be $0.13N^{-1/3}$ Å^{-1}, which is a quarter of the spacing of successive shells.

In experimental situations the smearing width has actual physical significance in terms of a characteristic temperature of the system under investigation. For example, a proper treatment of the effect of shells on the abundance spectra requires the introduction of a width of the order of the temperature. We discuss this temperature effect in Sec. VI. In the present section the width is included merely to visualize the shell and supershell structures.

The calculated level densities $\rho(E)$ are shown in Figs. 2(a), 2(b), and 2(c) for $N=1000$, 2000, and 3000, respectively. The wave number k_f corresponding to the Fermi energy is 0.89 Å^{-1}. In addition to the equidistant shell minima, the supershell structure, which is an envelope of the shell peaks, is clearly seen in these figures. For $N=1000$ the first node of the supershell is located at the Fermi level k_f, and moves down gradually as N increases. For $2000\lesssim N\lesssim 3000$ there is an antinode at k_f, indicating enhanced shell effects in this mass region.

Level densities at the Fermi energy have direct importance for a number of measurable quantities, and we have calculated $\rho(E_f)$ for each cluster number up to 4800. Figure 3 exhibits the values of $\rho(E_f)$ obtained by smearing the individual levels by 0.08 eV ($\simeq$900 K). The representation in Fig. 3 provides an alternative way of viewing the shells and supershells exhibited in Fig. 2.

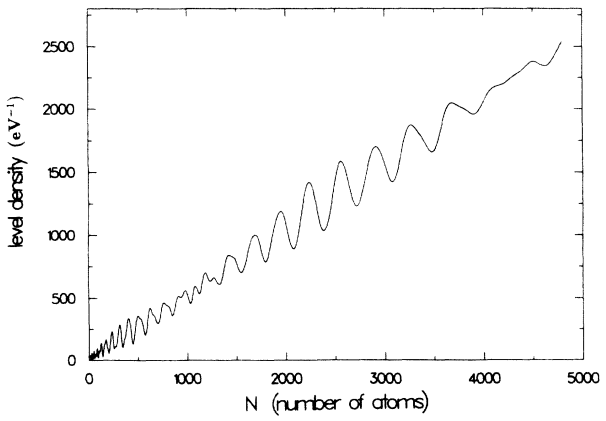

FIG. 3. Single-particle level densities at the Fermi energy in the Woods-Saxon potential. The smearing energy width is 0.08 eV. The Fermi energy is determined for each size N so that the integration of this level density up to the energy is equal to N.

In Sec. III B we shall compare these purely numerical results of the quantum calculations with the semiclassical theory of Balian and Bloch.

B. Semiclassical analysis

Deriving a semiclassical expression for the quantal level density in the spherical cavity in terms of a sum of contributions from different closed classical orbits, Balian and Bloch[11] were able to show that a supershell structure will emerge as a result of interference of amplitudes associated with classical triangular and square orbits. We investigate whether their interpretation of the supershells is also valid in the case of a Woods-Saxon potential.

There are several differences in the semiclassical expression for the level density between the cases of the spherical cavity with an infinitely high wall and of the smooth Woods-Saxon potential.[20] A convenient expression was derived for smooth spherical potentials by Berry and Tabor.[21] For the Woods-Saxon potential their expression reduces to

$$\rho(E)=\rho_{\rm TF}(E)+\sum_{\mathbf{M}}A_{\mathbf{M}}\cos\left[2\pi\mathbf{M}\cdot\left[\frac{\mathbf{I}_{\mathbf{M}}}{\hbar}-\frac{\alpha_{\mathbf{M}}}{4}\right]+\frac{\pi}{4}\right], \tag{3.3}$$

where the $\mathbf{M}$ is a vector of two positive (nonzero) integer components, M_l and M_s. Each set of M_l and M_s represents a classical closed orbit with M_l turns in the angular direction and M_s oscillations in the radial direction. The quantity $\mathbf{I}_{\mathbf{M}}$ is a set of two actions of the corresponding invariant torus with the frequency ratio $\omega_l/\omega_s=M_l/M_s$. The $\alpha_{\mathbf{M}}$ denotes the Maslov index associated with the closed orbit $\mathbf{M}$ [see Eq. (3.6)]. The amplitude $A_{\mathbf{M}}$ is positive for all values of M_l and M_s. The first term in Eq. (3.3) is the Thomas-Fermi average level density, which does not contribute to the shell structure.

The action term in the exponential is given as

$$2\pi\mathbf{M}\cdot\mathbf{I}_{\mathbf{M}}=\oint\mathbf{p}(\mathbf{r})\cdot d\mathbf{r}\ , \tag{3.4}$$

where the $\mathbf{p}(\mathbf{r})$ is the classical momentum of the particle which moves along a closed orbit, and the usual relation $\mathbf{p}=\hbar\mathbf{k}$ with the quantal wave vector is assumed. The magnitude of the momentum is given by

$$|\mathbf{p}(\mathbf{r})|=\{2m[E-U(r)]\}^{1/2}\ . \tag{3.5}$$

The integration in Eq. (3.4) is over one period of the closed orbit.

Equivalent to the smearing of the level energies, the $|\mathbf{k}(\mathbf{r})|$ is replaced by $|\mathbf{k}(\mathbf{r})|+ik_i$. When included in Eq. (3.3) this imaginary part of the wave number produces a suppression factor $e^{-k_iL_{\mathbf{M}}}$, where $L_{\mathbf{M}}$ is the trajectory length of the corresponding closed orbit.

A typical length of orbits turning around M_l times in the angular direction before they close is $2\pi M_lR_0=4.50\pi M_lN^{1/3}$ Å. As already stated, the value of k_i used in the quantum-mechanical calculation shown in Fig. 2 is $0.13N^{-1/3}$ Å^{-1}, and the suppression factor thus becomes $e^{-1.8M_l}$, which is a rapidly decreasing function of M_l. In the level-density calculation at the Fermi

TABLE I. Existing single-turn closed orbits in the Woods-Saxon potential. The calculation was made for $N=100,200,300,\ldots,$ up to 3000. The orbits are denoted by M_s, where the $M_s=2$ corresponds to a straight-line orbit through the center, and the $M_s=\infty$ orbit corresponds to the circle.

Number of atoms	M_s
$N<300$	$2,3,\infty$
$300\le N<800$	$2,3,4,\infty$
$800\le N<2200$	$2,3,4,5,\infty$
$2200\le N$	$2,3,4,5,6,\infty$

level shown in Fig. 3, the suppression factor is similar to the one stated above in the mass region $N\simeq 10^3$. We therefore consider only closed orbits with one turn ($M_l=1$) in the following.

Although all orbits are rounded off in a smooth potential, the single-turn orbits can still be identified by the numbers M_s. As a consequence we shall still denote the $M_s=3$ and 4 orbits by the triangular and square orbits, respectively, in analogy to the spherical cavity case.

Unlike the spherical cavity, there are only a finite number of single-turn orbits in the Woods-Saxon potential. The number increases as $\propto N^{1/6}$. The single-turn orbits near the Fermi energy, where the shell and supershell structures have the largest effects on observables, are listed in Table I for different intervals of N. Among the closed orbits in Table I the pendulating and circular orbits ($M_s=2$ and ∞, respectively) contribute to the level density only to higher order in $\hbar^{1/2}$. They have negligible contributions in the $\hbar\to 0$ limit.

Following Balian and Bloch we view the triangular ($M_s=3$) and square ($M_s=4$) orbits as responsible for the supershell structure in moderate-size clusters $N\lesssim 3000$.

The Maslov index in the smooth potential case is

$$\alpha_{\mathbf{M}}\cdot\mathbf{M}=2M_s+2M_l\ . \tag{3.6}$$

Defining

$$W_{M_s}=\frac{1}{\hbar}\mathbf{M}\cdot\mathbf{I}_{\mathbf{M}},\quad \text{where } \mathbf{M}=(1,M_s)\ , \tag{3.7}$$

the difference of the phase in Eq. (3.3) between the contributions of the triangular and square orbits is

$$\Delta\varphi=2\pi(W_3-W_4)-\pi\ . \tag{3.8}$$

When $\Delta\varphi=2n\pi$ (n is an integer) the two contributions add constructively, and when $\Delta\varphi=(2n+1)\pi$ they add destructively.

The difference $\Delta W=W_3-W_4$ was calculated at the Fermi energy for $100\le N\le 3000$. The result is shown in Fig. 4 where it can be seen that $\Delta W=1.0$ at $N\simeq 900$, indicating destructive interference and therefore a node of the supershell at the Fermi energy. The value of ΔW is 1.5 at $N\simeq 2200$, indicating a constructive sum of the amplitudes. The slope of the ΔW curve is less steep in the region $2000<N\lesssim 3000$, and therefore the antinode of the supershell will persist in a wide range of N. All the results of the semiclassical estimates are paralleled in the quantum-mechanical calculations as shown in Figs. 2 and 3.

For completeness we Fourier transformed the quantum-mechanical spectrum shown in Fig. 2 in order to confirm the dominance of the two closed orbits:

$$f(L)=\left|\sum_{nl}2(2l+1)k_{nl}^{-3/2}e^{ik_{nl}L}\right|\ . \tag{3.9}$$

We included single-particle levels from the lowest energy up to $E_{nl}<-2.5$ eV, slightly higher than the Fermi energy. We also transformed the smeared level density of Eq. (3.2) in order to show the effect of the smearing. For the convenience of display the absolute values are taken.

Figure 5 shows the results for $N=3000$. The solid and dashed curves are with and without the smearing, respectively. In both curves there are two prominent peaks, at lengths $L=171.2$ and 184.1 Å. In the Woods-Saxon potential they cannot be expected to exactly equal the trajectory lengths, but they should be very near to them. The corresponding triangular and square trajectory lengths in a spherical cavity with the radius $r_0N^{1/3}$ Å are 168.6 and 183.6 Å, respectively. The positions of the two peaks are thus very close to the lengths of triangular and

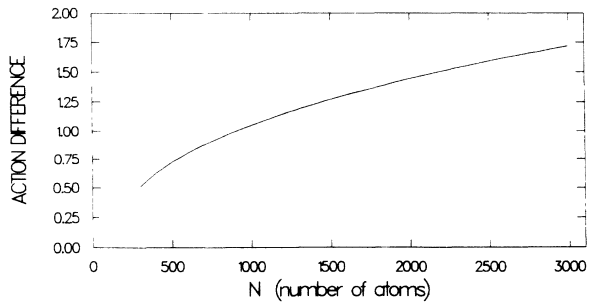

FIG. 4. The action difference ΔW between the triangular and square orbits in the Woods-Saxon potential.

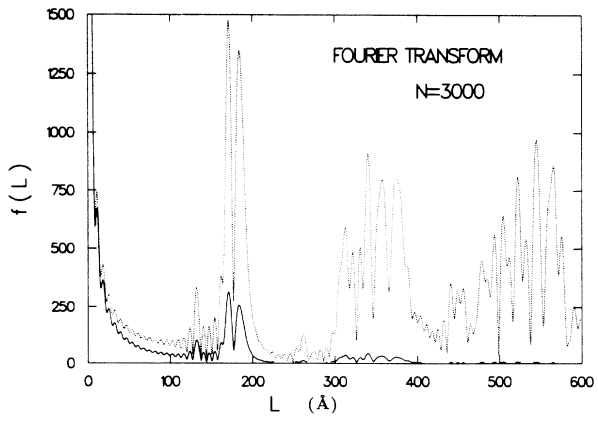

FIG. 5. Absolute values of Fourier components of the level energies in the Woods-Saxon potential with $N=3000$. The solid and dashed curves are with and without the smearing, respectively.

square orbits in the spherical cavity. This confirms that the interference of the two amplitudes associated with the two closed orbits is indeed the source of the supershell structure also for the case of the Woods-Saxon potential.

The difference of the phases of Eq. (3.9) between the two peaks at the Fermi energy is $(1/2\pi)k_{nl}(\Delta L)=(1/2\pi)0.89(184.1-171.2)=1.83$, which agrees within a reasonable accuracy with the semiclassical calculation of the phase difference ΔW, as shown in Fig. 4.

There are other smaller peaks in Fig. 5. They can all be identified with closed orbits. The peaks with larger L contribute to fine structures in the level density and are strongly suppressed in the solid curve for the smeared level density. The small peak at $L \simeq 130$ Å comes from the pendulating orbit.

IV. BINDING ENERGIES

The most direct experimental verification of the calculated electron eigenenergies would be based on spectroscopic experiments. At present such experiments are missing, except for quite small clusters. The mass spectroscopic measurements of cluster abundances, on the other hand, hinge on variations in separation energies of evaporated neutral atoms, and these variations also reflect the electronic shell effects. In the following we therefore calculate the shell oscillation part of the total binding energy of valence electrons in each cluster using the Woods-Saxon potential. We subsequently identify this part with the oscillating contribution to the total binding energy of the metal clusters.[22] The peaks in the abundance spectra correspond to particularly stable clusters, namely, to clusters which have larger binding energies than the clusters with neighboring masses.

We proceed as follows. For each N all single-electron energies E_j of the occupied states in the ground-state configuration are summed up. This sum is then divided into a smooth average part $E_{\rm av}$ and a shell part $E_{\rm shell}$:

$$E(N)=\sum_{j=1}^{N} E_j = E_{\rm av}(N)+E_{\rm shell}(N)\ . \tag{4.1}$$

The $E_{\rm av}$ is parametrized as consisting of a volume term ($\propto N$) plus a surface term ($\propto N^{2/3}$). The coefficients are obtained through a χ^2 fit to all $E(N)$ between 1 and 4800 leading to the result $E_{\rm av}=-4.34N+2.96N^{2/3}$ eV. When this is subtracted from the energy sum (4.1), the resulting $E_{\rm shell}$ is obtained as shown in Fig. 6. We note that the abscissa is not N itself but $N^{1/3}$. With this choice of scale the oscillations are equally spaced. The number of

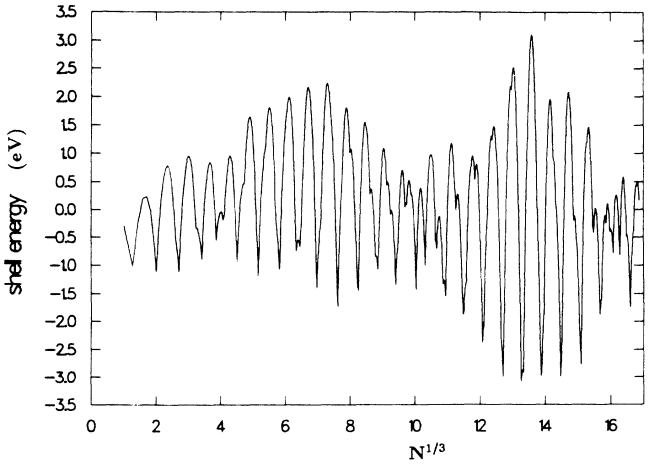

FIG. 6. The shell part of the total electronic binding energies of clusters as a function of $N^{1/3}$.

TABLE II. Minimum points of the shell energy as a function of the electron number. The pairs included in parentheses denote double minima which are close to each other.

Electron number N	Electron number $N^{1/3}$	Shell energy (eV)	Electron number N	Electron number $N^{1/3}$	Shell energy (eV)
2	1.26	−1.02	832	9.41	−1.35
8	2.00	−1.11	1012	10.04	−1.43
20	2.71	−1.12	1100	10.32	−1.00
40	3.42	−0.90	1216	10.67	−0.70
(58	3.87	−0.56	1314	10.95	−1.54
68)	4.08	−0.19)	1516	11.49	−1.87
92	4.51	−0.94	1760	12.07	−2.38
138	5.17	−1.19	2048	12.70	−3.00
198	5.83	−1.07	(2334	13.26	−3.08)
(254	6.33	−0.74	2368)	13.33	−2.92)
268)	6.45	−0.67)	2672	13.88	−2.99
338	6.97	−1.40	3028	14.47	−2.99
440	7.61	−1.74	3438	15.09	−2.77
562	8.25	−1.44	3848	15.67	−1.87
694	8.85	−1.07	4154	16.08	−0.78

different mass numbers included in one oscillation increases proportionally to $N^{2/3}$.

The minimum points in Fig. 6 represent the most stable spherical clusters, which are tabulated in Table II. The predicted stable clusters from 2 up to 138 were all observed in the measured abundance spectra. The magnitude of the E_{shell} is related to the quantity $\hbar\omega_{\text{sh}}\Omega$, where $\hbar\omega_{\text{sh}}$ is the energy distance between neighboring shells in the Fermi-energy region, and Ω is the effective number of degenerate levels in a shell.[10] In a spherical potential $\hbar\omega_{\text{sh}} \propto N^{-1/3}$ and $\Omega \propto N^{1/2}$. Therefore the magnitude of E_{shell} should increase as $N^{1/6}$. This roughly agrees with the overall tendency seen in Fig. 6.

There is however a very strong deviation from this overall dependence of $N^{1/6}$. It is due to the supershell structure. The envelope of E_{shell} has minima at $N \simeq 1000$ and 4000, maxima at $N \simeq 500$ and 2500. These mass numbers of diminished or enhanced E_{shell} exactly coincide with those at which the supershell structure in the level density has a node and an antinode, respectively, at the Fermi level. When E_{shell} is suppressed we do not expect to detect enhanced peaks in the abundance mass spectrum, and when E_{shell} is enhanced we do expect enhanced peaks. In this way the supershell structure is expected to reflect itself in experiment.

V. LEVEL DENSITIES IN THE "WINE-BOTTLE" POTENTIAL

The quantum-mechanical calculations of the level densities have also been made for a "wine-bottle" potential. As shown in Fig. 1, the potential is not entirely flat inside the surface, and the definition of the corresponding wave number by Eq. (3.1) is therefore not quite unambiguous. In order to compare with the case of the Woods-Saxon potential, we nevertheless use Eq. (3.1); with the value of V_0 chosen to be -5.95 eV. The magnitude of the imaginary momentum k_i is the same as before ($0.13N^{-1/3}$ Å^{-1}).

The results are shown in Figs. 7(a), 7(b), and 7(c) for $N=1000$, 2000, and 3000, respectively. At $N=1000$ the shell structure is enhanced compared to the Woods-Saxon case. At the Fermi level ($k_f=0.89$ Å^{-1}) there is an antinode of the supershell structure. At the $N=2000$ the shell structure is suppressed all over. There seems to be a node of the supershell structure near $k=0.6$–0.7 Å^{-1}, but it is not so clear as in the Woods-Saxon case. At $N=3000$ the supershell structure is clearly seen with a node at $k \simeq 0.75$ Å^{-1}.

We examine these variations of the level densities semiclassically. The semiclassical expression (3.3) is still valid provided that the eigenenergy is higher than the central ($R=0$) point of the potential ($\simeq -5.4$ eV). In the following we focus on the Fermi-energy region ($=-3.0$ eV).

The number of single-turn classical closed orbits is larger than in the Woods-Saxon case, as shown in Table III. This will make the interference of amplitudes associated with closed orbits more complicated. We therefore take into account three orbits ($M_s=3,4,5$) instead of two. The action W_{M_s} is defined by Eq. (3.7), and the

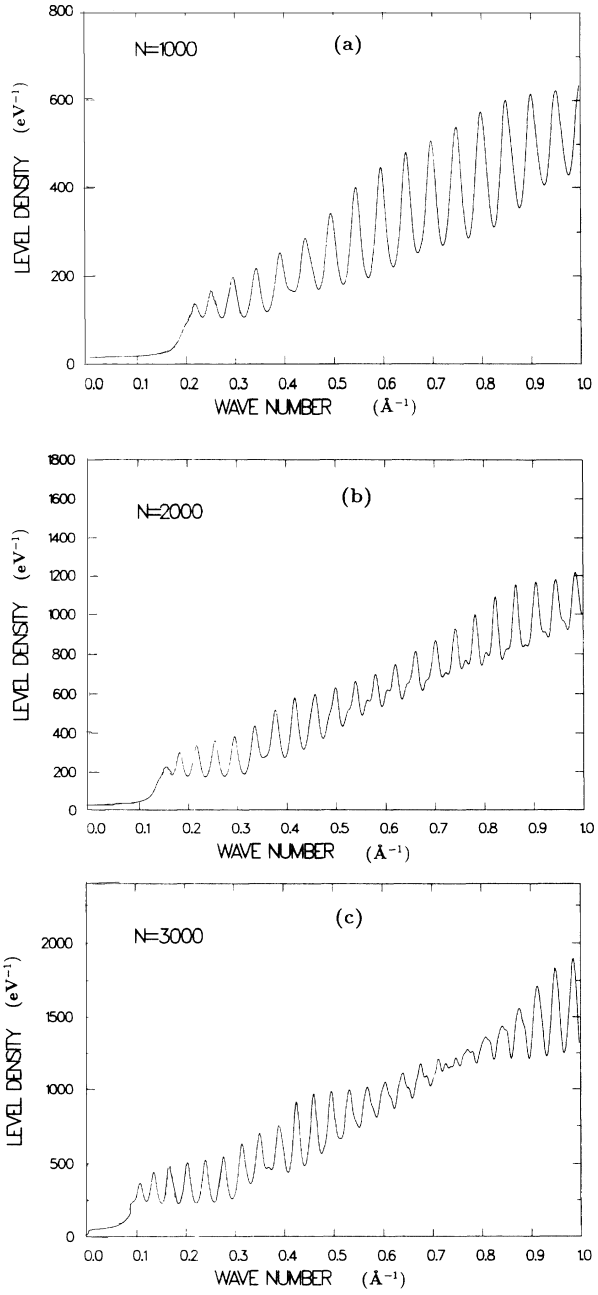

FIG. 7. Single-particle level densities in the wine-bottle potential with $N=1000$, 2000, and 3000 for (a), (b), and (c), respectively.

TABLE III. Existing single-turn closed orbits in the wine-bottle potential. See caption of Table I.

Number of atoms	M_s
$N<200$	2,3,4,5, ∞
$200\leq N<300$	2,3,4,5,6, ∞
$300\leq N<600$	2,3,4,5,6,7, ∞
$600\leq N<900$	2,3,4,5,6,7,8, ∞
$900\leq N<1500$	2,3,4,5,6,7,8,9, ∞
$1500\leq N<2500$	2,3,4,5,6,7,8,9,10, ∞
$2500\leq N$	2,3,4,5,6,7,8,9,10,11, ∞

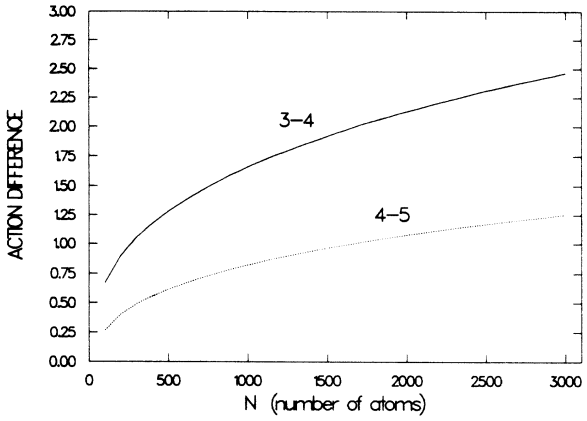

FIG. 8. The action differences in the wine-bottle potential; ΔW_{34} between the triangular and square orbits (upper solid curve), and ΔW_{45} between the square and pentagon orbits (lower dotted curve).

differences are defined as $\Delta W_{34}=W_3-W_4$ and $\Delta W_{45}=W_4-W_5$. As explained in Sec. III, when ΔW is an integer the interference is destructive, when ΔW is a half-integer it is constructive.

The action differences are shown in Fig. 8. The upper curve is for ΔW_{34}. It should have the dominant effect on the supershells. The quantity ΔW_{34} is 1.5 at $N\simeq 800$ and 2.5 at $N\simeq 3100$, at which mass numbers the interference is thus expected to be constructive. This prediction agrees with the quantum-mechanical results. [cf. Figs. 7(a) and 7(c)]. The value of ΔW_{34} is, on the other hand, 2.0 at $N\simeq 1600$ suggesting destructive interference. The lower curve in Fig. 8 shows ΔW_{45}, which also becomes 1.0 at $N\simeq 1600$. Since the curve of ΔW_{45} is very flat, the destructive interference of the square and pentagon orbits extends into the region $1000\lesssim N\lesssim 2500$. At $N\simeq 1600$ both of the interferences of the $M_s=3$ and 4 orbits and $M_s=4$ and 5 orbits are destructive, but this also means that the interference of the $M_s=3$ and 5 orbits is constructive. This complicated situation may be responsible for the obscuration of the supershell structure at $N=2000$ [cf. Fig. 7(b)].

VI. EFFECT OF FINITE TEMPERATURE ON SHELL STRUCTURE

In the molecular beam investigations of metal clusters it appears that the clusters are being studied at temperatures in the range of order 100 to 1000 K. In this range there are a number of different effects that will attenuate the energetic consequences of electronic shell structure. We shall in the following briefly consider (a) the thermal distribution of occupation probabilities for the electronic levels, (b) the scattering of electrons on the fluctuations of the positive ions, and (c) the effect of the thermal distribution of cluster shapes on the spectrum of electronic eigenvalues.

(a) The diffuseness of the Fermi distribution at $T\neq 0$ implies an evening out of the shell structure effect of electronic binding energies. This effect has been extensively discussed in connection with the studies of shell structure in excited nuclei (see, for example, Ref. 10, p. 607). The shell structure is associated with a "bunching" of electronic eigenvalues on an energy scale of order[23] $\hbar\omega_{\rm sh}\sim E_f/N^{1/3}$ (see Fig. 2). Thus, at temperature T the shell effect will be significantly reduced for cluster sizes exceeding

$$N^*\sim\left[\frac{E_f}{T}\right]^3 . \tag{6.1}$$

(b) A simple estimate of the electronic scattering on the fluctuations in the distribution of the positive ions can be based on the observed electrical resistivity ρ of the bulk metal. From the Drude formula we obtain the scattering lifetime

$$\tau=\frac{m}{e^2 n\rho} , \tag{6.2}$$

where m, e, and n are the mass, charge, and number density, respectively, for the electrons. Since the high-temperature resistivity of the metal (in both the liquid and solid forms) varies approximately linearly with the temperature the smoothing of shell structure due to scattering has a similar temperature dependence as that resulting from the distribution of occupation probabilities. Taking, for example, the observed high-temperature resistivity[24] of Na we have

$$\rho\simeq 3.0\times 10^{-8} T\ \Omega\,\text{cm} , \tag{6.3}$$

which implies a damping width Γ_ρ for each electronic level

$$\Gamma_\rho=\frac{\hbar}{\tau}\simeq 1.5T . \tag{6.4}$$

Thus the scattering of the electrons on the positive ions implies smoothing out of the electronic shell structure effects and limitation on cluster size that is numerically very close to the values (6.1) resulting from the distribution of occupation probabilities.

(c) For small clusters and low temperatures it is necessary to consider the effect on the shell structure resulting from the thermal fluctuations in the shape of the clusters. For small amplitude deviations from spherical shape we can expand the total energy of the electronic system in a power series in deformation parameters β,

$$V=\tfrac{1}{2}C\beta^2 , \tag{6.5}$$

with

$$C\sim NE_f \tag{6.6}$$

for configurations in the neighborhood of closed shells.[25] Thus at finite temperature we expect fluctuations in β of order

$$\Delta\beta\sim\left[\frac{T}{C}\right]^{1/2} . \tag{6.7}$$

These fluctuations are essentially static as compared with the characteristic periods in the electronic motion. In the

presence of static deformations particle orbits that were degenerate at $\beta=0$ are spread out over an energy interval of order

$$\Delta E \sim (\Delta\beta)E_f \sim \left[\frac{TE_f}{N}\right]^{1/2} . \tag{6.8}$$

The effect of the energy shifts (6.8) will be more important in smearing out the shell structure than the thermal damping effects discussed above if

$$\Delta E > T , \tag{6.9}$$

which gives a crossover at

$$N^* \sim \frac{E_f}{T} . \tag{6.10}$$

It appears that most studies of metal clusters carried out so far have involved temperatures of order a few hundred K and thus the crossover in these experiments would be at $N^* \sim 10^2$.

VII. SUMMARY

We have investigated shell and supershell structures in Na clusters. We assume a mean field for the valence electrons and simulate the mean field by two types of potentials (Woods-Saxon and wine-bottle potentials). In the Woods-Saxon potential the supershell structure is clearly recognized in the calculated level density of each cluster. Semiclassical consideration supports the interpretation of the supershell structure as coming from interference of amplitudes associated with triangular and square orbits. The shell part of the total binding energy for each cluster is also calculated as a function of the atom number N. The supershell structure is clearly reflected in the binding energy.

For the wine-bottle potential the supershell structure is also recognized in the level densities. But the nodes of the supershells appear at different wave numbers compared to the Woods-Saxon case. Moreover, the supershell pattern is not always a simple beating pattern of two waves. The reason for this complexity was investigated semiclassically, and it was found that other classical orbits (especially the pentagon orbit) have non-negligible contributions to the level densities in addition to the two most important orbits.

Although the Woods-Saxon and the wine-bottle potentials are similar to each other in shape, they produce level densities which contain different supershell structures. This means that the supershells are very sensitive to the details of the potential shape. The exact shell closings (magic numbers) are also sensitive to the potential shape.

We have also briefly considered thermal effects which tend to smooth out the shell-structure phenomenon. At the present time it does not appear that these effects will obscure the consequences of shell structure for cluster sizes up to several thousand atoms. There is an interesting crossover in the dominant mechanism for damping of single particle motion that is expected to occur for cluster sizes of order 100 atoms.

ACKNOWLEDGMENTS

We would like to express our sincere thanks to Sven Bjørnholm for stimulating discussions and encouragement through this work and also for reading through the manuscript and giving us useful comments and suggestions. We are grateful to Thomas Døssing, Matthias Brack, and Michael Hansen for discussions and assistance in computation. This work was supported by the Danish National Science Foundation.

[1]Proceedings of the Fourth International Meeting on Small Particles and Inorganic Clusters, Aix-en-Provence, 1988 [Z. Phys. D **12** (1989)].

[2]W. A. de Heer, W. D. Knight, M. Y. Chou, and M. L. Cohen, in *Solid State Physics*, edited by H. Ehrenreich, F. Seitz, and D. Turnbull (Academic, New York, 1987), Vol. 40, p. 93.

[3]W. D. Knight, W. A. de Heer, W. A. Saunders, M. Y. Chou, and M. L. Cohen, Phys. Rev. Lett. **52**, 2141 (1984).

[4]I. Katakuse, T. Ichihara, Y. Fujita, T. Matsuo, T. Sakurai, and H. Matsuda, Int. J. Mass Spectrom. Ion Phys. **67**, 229 (1985).

[5]Independently W. Ekardt had predicted the magic numbers theoretically by calculating the ionization potential and the mean binding energy per electron in Ref. 12.

[6]M. G. Mayer and J. H. D. Jensen, *Elementary Theory of Nuclear Shell Structure* (Wiley, New York, 1955).

[7]W. D. Knight, K. Clemenger, W. A. de Heer, and W. A. Saunders, Phys. Rev. B **31**, 2539 (1985).

[8]W. A. Saunders, K. Clemenger, W. A. de Heer, and W. D. Knight, Phys. Rev. B **32**, 1366 (1985).

[9]T. P. Martin (private communication); S. Bjørnholm (private communication).

[10]A. Bohr and B. R. Mottelson, *Nuclear Structure II* (Benjamin, New York, 1975), p. 578.

[11]R. Balian and C. Bloch, Ann. Phys. (N.Y.) **69**, 76 (1971).

[12]W. Ekardt, Phys. Rev. B **29**, 1558 (1984).

[13]D. E. Beck, Solid State Commun. **49**, (1984) 381.

[14]W. Kohn and L. J. Sham, Phys. Rev. **140**, A1133 (1965).

[15]N. D. Lang and W. Kohn, Phys. Rev. B **3**, 1215 (1971).

[16]W. Ekardt, Surf. Sci. **152**, 180 (1985).

[17]M. Brack, C. Guet, and H. Håkansson, Phys. Rep. **123**, 275 (1985); M. Brack, Phys. Rev. B **39**, 3533 (1989).

[18]This semiclassical approximation was tested for nuclei in Ref. 17 and was found to be valid for bulk properties of nuclei.

[19]Three parameters determine the numerical precision of the eigenvalues; the step size, the cutoff length, and the maximum accepted difference between the logarithmic derivative of the wave functions calculated outwards from $R=0$ and inwards from $R=R_{\max}$. With increments in N of 100 all three parameters were varied in order to check the convergence as well as the orthogonality of the wave functions. The values 0.05 Å and R_0+12 Å for the two lengths, and 10^{-6} for the third parameter gave precision of better than 10^{-3} eV.

[20]The semiclassical formulation of the level density in general form of potentials was first given by M. C. Gutzwiller in J. Math. Phys. **8**, 1979 (1967); **10**, 1004 (1969); **11**, 1791 (1970); **12**, 343 (1971).

[21]M. V. Berry and M. Tabor, Proc. R. Soc. London Ser. A **356**, 375 (1977).

[22]V. M. Strutinsky, Nucl. Phys. A **95**, 420 (1967).

[23]It should be emphasized that the characteristic energy spacing of the shells is much greater than the spacing E_f/N of the individual quantum levels. The recognition of important thermodynamic effects resulting from the discreteness of electronic levels on the latter energy scale was an early example of a "quantum size effect" in metal clusters (R. Kubo, J. Phys. Soc. Jpn. **17**, 975 (1962); L. P. Gor'kov and G. M. Eliashberg, Zh. Eksp. Teor. Fiz. **48**, 1407 (1965) [Sov. Phys.—JETP **21**, 940 (1965)]). But the experimental identification of these effects has proven illusive [W. P. Halperin, Rev. Mod. Phys. **58**, 533 (1986)].

[24]*Metals Reference Book*, 5th ed., edited by C. Smithells (Butterworths, London, 1976), p. 949.

[25]The estimate (6.7) assumes that the deformations are so small that the energy shifts (6.8) due to these deformations are small compared with the energy spacings of the shells, $\hbar\omega_{\rm sh} \simeq E_f N^{-1/3}$, which demands, for closed-shell configurations, $T \ll E_f N^{1/3}$, a condition that will always be well satisfied.